Material composition study and computational evaluation toward the fabrication of tubular positive electrodes for high-capacity lead-acid batteries

Dao The Nam[1*], Ninh Duc Ha[1], Doan Tuan Anh[1], Doan Minh Cuong[1], Nguyen Thi Huong[1], Vu Thi Thao[2], Vu Minh Thanh[1]

[1]Institute of Materials, Biology and Environment, Academy of Military Science and Technology, 17 Hoang Sam, Nghia Do, Hanoi, Vietnam;
[2]VNU University of Engineering and Technology, 144 Xuan Thuy, Nghia Do, Hanoi, Vietnam
[*]Corresponding author: namke@mail.ru
Received 9 Aug. 2025; Revised 03 Oct. 2025; Accepted 16 Oct. 2025; Published 18 Nov. 2025.
DOI: https://doi.org/10.54939/1859-1043.j.mst.101.2025.200-206

ABSTRACT

This study investigates the material composition and structural characteristics of tubular positive electrodes in high-capacity lead–acid batteries, combining experimental analysis with theoretical design calculations. Advanced characterization techniques, including X-ray diffraction (XRD), scanning electron microscopy coupled with energy-dispersive X-ray spectroscopy (SEM–EDS), and infrared (IR) spectroscopy, were employed to identify phase composition, elemental constituents, and organic additives. Results indicate that the positive active mass primarily consists of tetragonal PbO_2 with minor orthorhombic $PbSO_4$, along with carbonaceous and polymeric conductive additives. The tubular sheath was found to be a polyester-based composite containing ester, alcohol, and anhydride functional groups, with silica-derived Si–O–Si structures. SEM analysis revealed a highly porous fine-particle morphology, suitable for binder-free filling into tubular casings. Computational design determined key structural and mass parameters of the positive active material (PAM), leading to an optimized electrode configuration with a theoretical battery capacity of 17,189 Ah. These findings provide a scientific basis for the domestic production of high-performance tubular lead–acid batteries.

Keywords: Tube electrode; PAM; Lead-acid battery.

1. INTRODUCTION

Lead–acid batteries with tubular positive plates are extensively employed in industrial and heavy-duty applications owing to their high charge acceptance and extended cycle life. Many high-performance designs currently available in the global market are the result of decades of proprietary research and optimization by leading manufacturers. These imported products often exhibit superior electrochemical characteristics due to finely tuned material formulations, advanced grid alloys, and specialized tubular structures. However, the lack of accessible technical documentation or technology transfer presents significant barriers to domestic production efforts.

In this context, decoding the material composition, structural architecture, and functional behavior of such foreign-manufactured tubular electrodes becomes a critical step toward the development of equivalent or improved lead–acid batteries within domestic industries. Advanced characterization techniques, including XRD, SEM-EDS, Raman spectroscopy, and electrochemical impedance spectroscopy, enable a detailed understanding of the phase composition, additive systems, and microstructural features embedded in these commercial electrodes [1]. Simultaneously, theoretical modeling and simulation approaches, ranging from density functional theory (DFT) to continuum-scale electrode modeling, play a vital role in predicting material performance, failure mechanisms, and guiding the design of optimized electrode systems tailored to local production capabilities [2-5].

A combined strategy integrating experimental decoding and theoretical calculations is therefore essential not only to reverse-engineer advanced battery systems but also to lay the scientific and technological foundation for a self-reliant, high-quality domestic manufacturing chain.

2. EXPERIENCE

2.1. Calculated parameters of active materials for electrodes

The active materials formed in the two types of electrodes consist of two structural components:

Energy structure, Ge: This participates directly in the discharge process.

Skeletal structure, Gs: This provides mechanical support to the energy structure and possesses electrical conductivity, thereby enabling current conduction throughout the electrode plate volume.

The total mass (G) of the positive or negative active material in a cell is given by: $G = Ge + Gs$.

All calculations of active materials are performed using the value of G. There are three key parameters used to define the specific capacity.

2.1.1. Active material utilization coefficient (η)

This coefficient represents the mass fraction of the energy structure within the total mass of the positive or negative active material in a single cell: $\eta = Ge / G$, $\eta < 1$.

The mass of NAM (Negative Active Material) or PAM (Positive Active Material) per cell for a given capacity (C) is calculated as follows: $Ge = C \cdot \delta_0$; $G = C \cdot \delta_0 / \eta$ $[g \cdot cell^{-1}]$.

The physical significance of the active material utilization coefficient is straightforward, it indicates the fraction of the total active material that actually participates in generating and storing electrical current.

2.1.2. Mass coefficient of active material per ampere-hour (β)

This coefficient quantifies the actual amount of PAM or NAM (in grams) required to deliver 1 Ah of capacity during discharge. $\beta = G / C$ $[g \cdot Ah^{-1}]$. The β value is empirically determined for each specific manufacturing technology of the positive or negative electrode active material. It also depends on the battery type.

2.1.3. Specific capacity of PAM or NAM per kilogram of active material (σ)

This is the reciprocal of β: $\sigma = C / G$ $[Ah \cdot kg^{-1}]$. It represents the ampere-hours that can be delivered by 1 kg of PAM or NAM.

2.2. Research methods

For IR measurements, the active material samples were rinsed with distilled water to remove residual acid and air-dried. The positive grid samples were cleaned by scraping off attached active material, washed with distilled water, and subjected to ultrasonic treatment for 15 minutes to eliminate remaining residues, followed by rinsing, drying, and subsequent IR analysis.

For SEM–EDX analysis, the positive active material was carefully separated from the grid, repeatedly rinsed with distilled water to remove residual acid, ultrasonically treated for 15 minutes, rinsed again, and air-dried prior to measurement.

The morphology and elemental composition of the active material were investigated using Scanning Electron Microscopy (SEM) and Energy Dispersive X-ray Spectroscopy (EDS), performed with a JEOL JSM–IT800 system at the University of Science and Technology of Hanoi.

The phase composition of the material was analyzed using the XRD method on an X'Pert system at the University of Science and Technology of Hanoi.

The organic composition of the material was evaluated using infrared spectroscopy on a Bruker instrument at the Institute of Materials, Biology, and Environment.

3. RESULTS AND DISCUSSION

3.1. Analysis of the positive plate structure

The positive electrode in the investigated battery is of the tubular type (table 1), with the specifications listed below:

***Table 1**. Selected specifications of the tubular positive electrode.*

No.	Parameter	Value
1	Number of plates	36
2	Dimensions (length × width × thickness), mm	910 × 330 × 9
3	Number of current collector rods per plate	34
4	Mass of active material in one tube, g	~170
5	Length of current collector rod, mm	900
6	Diameter of current collector rod, mm	3

The positive plate is fabricated in a tubular configuration. The tubular active material is enclosed in individual woven cylindrical sleeves, connected in parallel through a top busbar to form a single plate. The tubes are of circular cross-section, with their bottoms sealed by plastic plugs. Each plate consists of 34 tubes with a diameter of 9 mm, and the woven sleeves are joined together.

The tubular electrode design improves upon flat plate electrodes in two main aspects: The mass of the current collector is reduced, increasing the proportion of active material, thereby enhancing the battery's capacity. The tube casing and bottom plugs prevent the active material from shedding during operation, thereby extending battery life and reducing the risk of short-circuiting caused by active material deposition at the bottom of the battery. The current collector consists of slender rods running centrally along each tube, with a diameter of 3 mm, welded at one end to the support bar, similar to the negative plate configuration.

3.2. Material composition analysis of the positive electrode

Composition analysis of the positive current collector

A sample of the positive current collector was mechanically cleaned with 2000-grit sandpaper, flattened, and analyzed via XRD. The XRD pattern (figure 1) shows major diffraction peaks at 2θ values of 31.26°, 36.30°, 52.24°, 62.17°, and 65.21°, corresponding to the standard cubic crystal planes of lead: (111), (200), (220), (311), and (222).

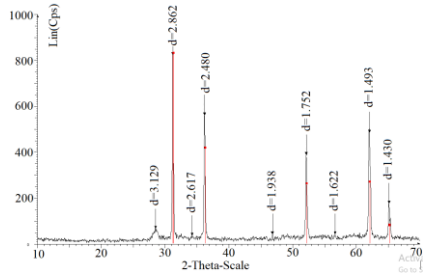

***Figure 1.** XRD spectrum of the anode collector plate.*

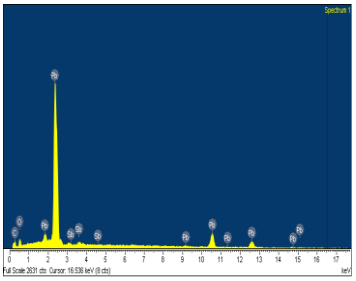

Element	Weight%
C K	5.07
O K	9.96
Sb L	2.25
Pb M	82.72
Totals	100.00

***Figure 2.** EDS spectrum of the anode collector plate.*

Typically, lead current collectors are fabricated from lead–antimony or lead–calcium alloys to enhance castability. If the alloying content is low, it may not be clearly detected by XRD.

EDS analysis was performed for further confirmation. At different points on the current collector surface, the main elements detected were Pb and Sb, with an average antimony content of approximately 2%. Oxygen originates from lead oxide in the active mass, which is primarily lead(II) oxide. The detection of Sb suggests that the current collector was produced by molten casting.

Historically, Pb–Sb alloys for positive current collectors contained up to 11–13% Sb [5]. However, later studies demonstrated that high Sb content increases Sb migration from the positive to the negative plate, creating numerous local discharge sites on the negative plate, leading to overheating, high water loss, and increased explosion risk [6, 7]. Moreover, due to Sb's toxicity, its content in lead alloys has been progressively reduced; in modern lead–acid batteries, Sb content

typically ranges from 1–3%. Given the considerable length of the collector rods, 2% Sb is used to improve mechanical properties [8], minimizing warping and breakage during active mass filling.

Optical emission spectroscopy was also employed to confirm elemental composition. The Sb content of ~ 2.3% closely matches the EDS results.

Table 2. *Elemental composition of the anode collector plate according to the EOS spectrum.*

Element	Sn	Sb	Al	Bi	Cu	Fe
%	0,2184	2,3369	0,0013	0,0035	0,0315	0,0010
Element	As	Te	Ni	Se	S	P
%	0,1866	0,0027	0,0008	0,0570	0,0047	97,7317

Thus, combining results from different methods, it can be concluded that the positive current collector is made of lead–antimony alloy containing approximately 2–2.3% Sb, produced by casting.

3.3. Composition analysis of the positive active material

The main component of positive active mass is typically red lead (lead(IV) oxide). EDS analysis of the positive active material revealed Pb, O, Al, and C as the primary elements.

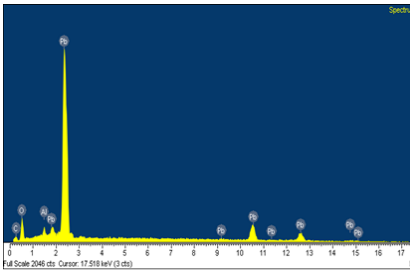

Element	Weight%
C K	2.78
O K	18.16
Sb L	1.01
Pb M	78.05
Totals	100.00

Figure 3. *EDX spectrum of the PAM.*

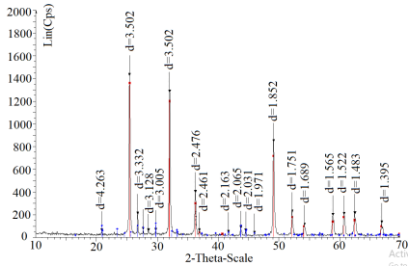

Figure 4. *XRD spectrum of the PAM.*

The results obtained from different locations of the positive active material indicate that its main elemental constituents are Pb, O, Al, and C. This composition is highly consistent with the presence of lead dioxide and aluminum oxide in the positive active mass. As for carbon, similar to the negative active material, it may originate from two possible sources: carbon powder or organic additives.

To further elucidate the composition of the positive active material, XRD analysis of the powder was conducted. In the XRD pattern (figure 4), two distinct peak groups matching reference spectra are observed. The first group, highlighted in red, corresponds to diffraction angles characteristic of tetragonal PbO_2, comprising multiple peaks with high intensity and narrow widths, indicative of a high degree of crystalline order. The second group, marked in blue, exhibits diffraction angles consistent with orthorhombic $PbSO_4$; The peaks in this group have relatively low intensity, most likely due to the low content of $PbSO_4$.

To determine the presence of organic additives in the positive active material, IR spectroscopy was performed on the active material powder after it had been thoroughly washed with distilled water and dried at ambient temperature. From the spectrum in figure 5, several observations can be made. A cluster of closely spaced bands in the wavenumber range 1600 - 2000 cm^{-1}, with weak intensities, is characteristic of vibrational modes associated with aromatic ring compounds containing substituted groups on the outer ring. The bands at 1282 cm^{-1} and 1160 cm^{-1} are characteristic of C–O–C stretching vibrations in esters, with the 1282 cm^{-1} band specifically corresponding to esters of aromatic acids. The peak at 750 cm^{-1}, of relatively low intensity, is consistent with δ_{N-H} bending vibrations in higher-order amides. Carbonaceous species, improved electronic percolation and nucleation control of PbO_2; ester/amide-type organics, binder/anti-shedding functions, wetting modification, and microstructural stabilization during sulfate–oxide transformations; and crystal-habit/porosity regulation that affects sulfate formation and charge transfer.

Combining these spectral features suggests a composition closely resembling an ester of polyhydroxy acid (PHA) containing amide groups. Such compounds are also known to be used as conductive additives in positive active materials. The presence of the band at 979 cm^{-1} indicates δ_{C-H} out-of-plane vibrations associated with the trans isomer HRC=CR'H, while the band at 846 cm^{-1} is characteristic of δ_{C-H} out-of-plane vibrations bonded to higher-order carbon atoms in RR'C=CR''H linkages. Thus, the positive active material also contains organic compounds serving as additives.

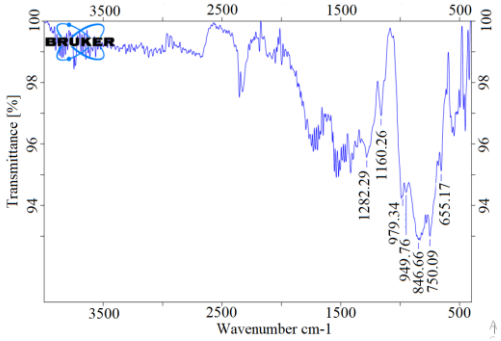

Figure 5. *IR spectrum of the PAM.*

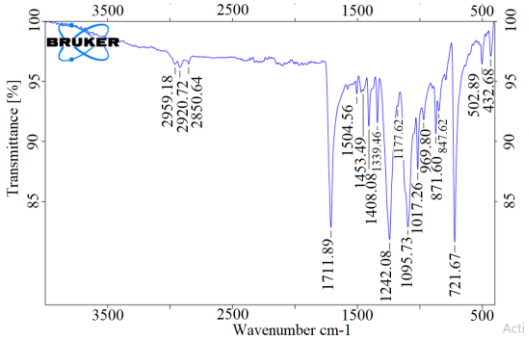

Figure 6. *IR spectrum of the tubular sheath of the positive electrode.*

The tubular sheath of the positive electrode was thoroughly washed several times with distilled water, then dried at ambient temperature, and subsequently analyzed by IR spectroscopy. The tubular sheath of the positive electrode was thoroughly washed several times with distilled water, dried at ambient temperature, and subsequently analyzed by IR spectroscopy, with the results shown in figure 6. A strong absorption band at 1712 cm^{-1} is characteristic of C=O stretching vibrations in unsaturated esters; the band at 1408 cm^{-1} corresponds to deformation vibrations of aromatic rings. Peaks at 1339 cm^{-1} and 1018 cm^{-1} are associated with vibrations in carboxylic ester or aldehyde groups; Specifically, the 1018 cm^{-1} band indicates the presence of O=C–O–C linkages or secondary alcohols. The band at 969 cm^{-1} corresponds to C=C stretching vibrations, while the peak at 869 cm^{-1} suggests a benzene ring substituted with five hydrogen atoms.

Combining these spectral features suggests that the sheath material is primarily a polyester containing ester, alcohol, anhydride, aromatic, and heteroaromatic ring structures. The presence of carboxyl, ester, anhydride, and hydroxyl groups indicates that the polyester fabric is not pure PET. The peak at 1408 cm^{-1}, corresponding to aromatic ring vibrations, is a stable characteristic feature of PET, while the 1712 cm^{-1} band is assigned to ester groups. Additionally, two characteristic peaks of Si–O–Si vibrations were detected at approximately 847 cm^{-1} and 1095 cm^{-1}, attributed to Si–O bending and asymmetric Si–O–Si stretching modes, respectively.

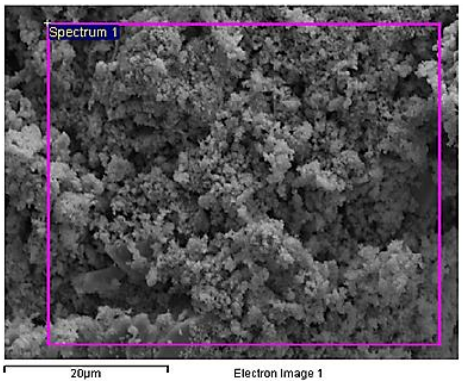

Figure 7. *SEM image of the active anode.*

The morphology of the anode active substance was observed by scanning electron microscopy (figure 7). Observing the SEM image, it can be seen that the anode has a structure of very small, very porous particles and does not form flocculent patches. From this, it can be seen that the anode can be put into the electrode tube in the form of dry powder and can be put without using a binder. This is also an advantage of the tube electrode when not using a binder, but still keeping the active substance on the electrode.

3.4. Calculation of the mass of PAM

The electrochemical equivalent of PbO_2 per ampere-hour is $\delta^0_{PbO2} = 4{,}463\ g\ PbO_2\ Ah^{-1}$. For the sample battery, the required capacity is C=17000 Ah.

$$G^e_{PbO2} = 17.000 \times 4{,}463 = 75.871\ g\ PbO_2$$

This energy structure of the PAM participates in the electrochemical discharge reaction. To calculate the total mass of the PAM, it is also necessary to account for the skeletal structure of the PAM, which does not participate in the reaction. The total mass of PAM (G) at a utilization coefficient of η_{PAM} = 0.33 [10] can be determined by dividing the mass of the PAM's energy structure by the utilization coefficient: $G_{PAM} = 75.871/0{,}33 = 229.912\ g\ PAM.cell^{-1}$.

Mass coefficient of active material per Ah, (β_{PbO2}): $\beta_{PAM} = 229.912/17.000 = 13{,}52$ [g PAM.Ah^{-1}]. Combining the parameters obtained from the above investigations, a design calculation table for the sample battery is established (table 3).

Table 3. *Calculated parameters for the sample electrode.*

Parameter	Unit	Symbol	Calculation formula	Value
Energy density of the active material	g/Ah	β		13,52
Apparent density of the active material	g/cm^3	ρ		4,2
Diameter of the electrode spine rod	cm	*d*		0,30
Inner diameter of the tube	cm	*D*		0,85
Cross-sectional area of the active material in a single tube	cm^2	*A*	$A = \pi*(D^2-d^2)/4$	0,497
Length of a single tube	cm	*l*		91
Volume of active material in a single tube	cm^3	*v*	*v = A*l*	45,21
Mass of active material in a single tube	g	*m*	m = ρ*v	189,86
Number of tubes per electrode plate		*n*		34
Total tube length per electrode plate	cm	*L*	*L = l*n*	3.094
Total volume of active material per electrode plate	cm^3	V	V = A*L	1.537
Total mass of active material per electrode plate	g	M	M = ρ*V	6.455
Number of positive electrode plates in a battery		N		36
Total mass of active material in a battery	g	G	G = M*N	232.393
Theoretical capacity of a single electrode plate	Ah	c	c = M/β	477
Theoretical capacity of a battery	Ah	C	C = G/β	17.189

The theoretical design calculations will help optimize the method of introducing the active material into the electrode tubes in order to achieve the desired capacity.

4. CONCLUSIONS

The combined experimental–computational approach successfully identified the phase composition, microstructure, and organic additives of tubular positive electrodes, and established key design parameters for high-capacity lead–acid batteries. The results confirm the feasibility of binder-free PAM utilization, highlight the functional role of polyester–silica composite sheaths, and deliver a validated design yielding a theoretical capacity consistent with industrial performance targets. This work lays the groundwork for localized manufacturing of advanced tubular lead–acid battery systems.

Acknowledgment: *The authors thank the funding of the project DTDLCN6623.*

REFERENCES

[1]. Li, M., Zhao, Y., & Chen, D., *"Advanced Characterization of Tubular Lead–Acid Battery Electrodes for Material Reconstruction and Performance Benchmarking"*, Journal of Energy Storage, Vol. 76, 109325, (2024).

[2]. Nguyen, H. T. et al., *"Computational Modeling for Optimization of Lead–Acid Battery Electrodes: Toward Domestic Manufacturing Strategies"*, Electrochimica Acta, Vol. 445, 141030, (2023).

[3]. Nazghelichi, T., Torabi, F., & Esfahanian, V., *"Non-dimensional analysis of electrochemical governing equations of lead–acid batteries"*, (2017).

[4]. Sunu, W. G., *"Mathematical Model for Design of Battery Electrodes: Lead-Acid Cell Modelling"*, in Electrochemical Cell Design, (1984).

[5]. Sulzer, V., Chapman, S. J., Please, C. P., Howey, D. A., & Monroe, C. W., *"Faster Lead-Acid Battery Simulations from Porous-Electrode Theory: II. Asymptotic Analysis"*, (2019).

[6]. Habashi, F., *"Alloys: Preparation, Properties, Applications"*, 1st Ed, Wiley-VCH, New York, (1998).

[7]. Clark, M. S., *"Lead-antimony, lead-calcium, lead-selenium, VRLA, Ni-Cd"*, paper presented at the International Stationary Battery Conference, Gaylord Palms Resort and Convention Centre, Orlando, Florida, USA, 26–29, (2009).

[8]. Liu, J., Li, X., Barbero, E., & Dong, C., *"Effect of Sn concentration on the corrosion resistance of Pb–Sn alloys in H_2SO_4 solution"*, Journal of Power Sources, Vol. 155, No. 2, pp. 420–427, (2006).

[9]. Guruswamy, S., *"Engineering Properties and Applications of Lead Alloys"*, 1st Ed, Marcel Dekker, (2000).

[10]. Prout, L., *"Aspects of lead/acid battery technology 2. Tubular positive plates"*, Journal of Power Sources, Vol. 41, pp. 163–183, (1993).

TÓM TẮT

Nghiên cứu khảo sát thành phần vật liệu và tính toán định hướng chế tạo điện cực dương dạng ống của ắc quy chì-axit dung lượng cao

Nghiên cứu này tập trung vào điện cực dương dạng ống trong ắc quy chì–axit dung lượng cao, kết hợp giữa phân tích đặc trưng thực nghiệm và tính toán thiết kế lý thuyết. Các kỹ thuật phân tích tiên tiến, bao gồm nhiễu xạ tia X (XRD), hiển vi điện tử quét kết hợp phổ tán sắc năng lượng tia X (SEM–EDS) và quang phổ hồng ngoại (IR), được sử dụng để xác định thành phần pha, thành phần nguyên tố và các phụ gia hữu cơ. Kết quả cho thấy chất hoạt động cực dương chủ yếu gồm PbO_2 dạng tetragonal với một lượng nhỏ $PbSO_4$ dạng orthorhombic, cùng với các phụ gia dẫn điện có nguồn gốc cacbon và polyme. Phần vỏ ống được xác định là vật liệu composite nền polyester chứa các nhóm chức este, rượu và anhydrit, cùng với liên kết Si–O–Si có nguồn gốc từ silica. Phân tích SEM cho thấy cấu trúc vi mô hạt mịn, độ xốp cao, phù hợp cho công nghệ nhồi bột khô vào ống. Tính toán thiết kế đã xác định các thông số cấu trúc và khối lượng chủ chốt của chất hoạt động điện cực dương (PAM), từ đó tối ưu hóa cấu hình điện cực với dung lượng lý thuyết đạt 17.189 Ah. Các kết quả này cung cấp cơ sở khoa học vật liệu vững chắc cho việc nội địa hóa sản xuất ắc quy chì–axit dạng ống hiệu suất cao.

Từ khoá: Ắc quy chì-axit; Điện cực ống; PAM.